Journal of Nuclear Medicine, published on January 19, 2023 as doi:10.2967/jnumed.122.264981

Consecutive PSMA and AR PET imaging shows positive correlation to AR and PSMA protein expression in primary hormone naïve prostate cancer.

Valentin al Jalali[1,2], Gabriel Wasinger[3], Sazan Rasul[4], Bernhard Grubmüller[5], Beatrix Wulkersdorfer[1, 2], Theresa Balber[1,4], Markus Mitterhauser[1, 4, 6], Judit Simon[1, 7], Marcus Hacker[4], Shahrokh Shariat[8], Gerda Egger[1, 3, 9], Markus Zeitlinger[1, 2]#

[1]Ludwig Boltzmann Institute Applied Diagnostics, Austria

[2]Department of Clinical Pharmacology, Medical University of Vienna, Austria

[3]Department of Pathology, Medical University Vienna, Austria

[4]Department of Biomedical Imaging and Image guided Therapy, Division of Nuclear Medicine, Medical University Vienna, Austria

[5]Department of Urology and Andrology, University Hospital Krems, Karl Landsteiner University of Health Sciences, Krems, Austria

[6]Institute of Inorganic Chemistry, Faculty of Chemistry, University of Vienna, Austria

[7]Department of Health Economics, Center for Public Health, Medical University of Vienna, Austria

[8]Department of Urology, Medical University Vienna, Austria

[9]Comprehensive Cancer Center, Medical University of Vienna, Vienna, Austria

Corresponding author:

Markus Zeitlinger, MD

Department of Clinical Pharmacology

Vienna University Hospital

Mailing address: Medical University of Vienna, Waehringer Guertel 18-20, 1090 Vienna, Austria

Phone: +43-1-40400-29810

Fax: +43-1-40400-29980

E-mail: markus.zeitlinger@meduniwien.ac.at

http://www.meduniwien.ac.at/klpharm/

First author:

Valentin al Jalali, MD; medical resident

Department of Clinical Pharmacology

Vienna University Hospital

Mailing address: Medical University of Vienna, Waehringer Guertel 18-20, 1090 Vienna, Austria

Phone: +43-1-40400-29810

Fax: +43-1-40400-29980

E-mail: valentin.aljalali@meduniwien.ac.at

Word count: 3099 words

Short running title: PSMA and AR in prostate cancer

ABSTRACT

Rationale: The present study set out to investigate if PET imaging can be used as a potential substitute for immunohistochemical analysis of tumor samples in prostate cancer (PC) patients. Correlation between imaging signals of two PET tracers and the corresponding target structures was assessed. The first tracer was [^{68}Ga]Ga-PSMA$^{HBED-CC}$([68Ga]PSMA), which is already implemented in clinical routine. The second tracer was [^{18}F]-fluoro-5α-dihydrotestosterone([18F]FDHT) which binds to the androgen receptor (AR). The AR is particularly interesting in PC, since the AR expression status and its shift during therapy might directly influence patient care.

Methods: This prospective, explorative clinical study included 10 newly diagnosed PC patients. Each patient received a [68Ga]PSMA-PET/MRI- and [18F]FDHT-PET/MRI-scan prior to prostatectomy. Cancer standardized uptake values (SUV) were determined and related to background SUVs. Following prostatectomy, tumor tissue was sampled and AR and prostate-specific membrane antigen (PSMA) expression determined. AR and PSMA expressions were evaluated quantitively with QuPath and additionally with a four-tiered rating system. Correlation between imaging signals and marker expression was statistically assessed.

Results: For [18F]FDHT, the $SUV_{max}/SUV_{background}$ ratio showed a significant, strong correlation (P-value=0.019, r=0.72) with AR optical density of the correlating tissue sample. The correlation between PSMA optical density and the [68Ga]PSMA $SUV_{max}/SUV_{background}$ ratio was not significant (P-value=0.061), yet a positive correlation trend could be observed (r=0.61). $SUV_{max}/SUV_{background}$ ratios were higher for [68Ga]PSMA

(34.9±24.8) compared to [18F]FDHT (4.8±1.2). In line with this findings, the tumor detection rate of the Ga-PSMA-PET scan was 90%, but only 40% for the [18F]FDHT-PET scan. The four-tiered rating of PSMA staining intensity yielded very homogenous results with values of 3+ for most subjects (90%). The AR staining was rated with 1+ in two patients (20%), with 2+ in four patients (40%) and with 3+ in four patients (40%).

Conclusion: [18F]FDHT-PET may be useful for monitoring AR expression and alterations of AR expression during treatment of PC patients. This may facilitate early detection of treatment resistance and allows for adaptation of therapy to prevent cancer progression. [18F]FDHT-PET is inferior to [68Ga]PSMA-PET for primary PC diagnosis, but the correlation between [68Ga]PSMA SUVs and PSMA expression is weaker compared to [18F]FDHT and the AR.

Key words: PSMA PET, FDHT PET, AR protein expression, PSMA protein expression, primary hormone naïve prostate cancer

INTRODUCTION

Prostate cancer (PC) is causing significant mortality and morbidity worldwide and accounts for approximately 3.8% of deaths caused by cancer in men (*1*). Although novel diagnostic and therapeutic options led to a decrease in PC related mortality, the incidence of PC is increasing (*2*).

The androgen receptor (AR) plays a central role in PC development and progression (*3,4*). Multiple therapies for PC target the hormonal axis connected to the AR (*5*). Therefore, information on AR expression status and its shift during therapy and along the treatment course would possibly allow prediction of treatment response and imminent resistance to therapy (*6*).

[18F]-fluoro-5α-dihydrotestosterone (FDHT) binds to the AR and has been discussed to be particularly useful in deciphering the role of the AR in resistant and progressive metastatic PCs (*7*). Fox et al. performed [18F]FDHT- and [18F]-fluoro-2-D-deoxyglucose (FDG)-PET scans on 133 metastatic castration resistant PC patients in a prospective clinical study. The authors were able to demonstrate that PET-based assessment of AR expression with [18F]FDHT and glycolytic activity with [18F]FDG can detect tumor heterogeneity impacting survival (*7*). Data on [18F]FDHT kinetics are limited to castration resistant PC patients and its use as an imaging agent is still restricted to clinical studies and has not been applied in clinical routine (*8,9*).

In contrast, the clinical utility of [^{68}Ga]Ga-PSMA$^{HBED-CC}$ ([68Ga]PSMA)-PET has been widely accepted and it is regularly used in routine clinical practice for primary

detection of PC and in recurrent disease (*10,11*).

Few clinical studies are available linking histopathologic patterns in tumor tissue to imaging signals (*7,12,13*). To date, there are no studies published that have quantitatively analyzed whether PET-based assessment of AR and prostate-specific membrane antigen (PSMA) expression in PC correlates with histopathological expression of these markers. However, this knowledge is essential to reliably assess tumor heterogeneity and monitor alterations of AR and PSMA during therapy using non-invasive PET scans as a potential substitute for histopathological analysis via repeated biopsies.

The present study aimed to investigate if PET imaging can be used as a substitute for immunohistochemical analysis of tumor samples in patients with newly diagnosed PC. For this purpose, [68Ga]PSMA- and [18F]FDHT-PET images were correlated with AR and PSMA immunohistochemical expression in PC tissue.

MATERIALS AND METHODS

Ethics

This study was conducted at the Medical University of Vienna (Austria) and the Ludwig Boltzmann Institute Applied Diagnostics (Austria) in accordance with the Declaration of Helsinki and the Good Clinical Practice Guidelines of the International Conference on Harmonization. The study was approved by the Ethics Committee of the Medical University of Vienna. Before inclusion, all study subjects gave oral and written informed consent to study participation.

Trial Design and Study Population

The present study was designed as a prospective, explorative clinical study. A total of 10 patients with newly diagnosed PC were included. Main inclusion criteria were age ≥ 18 years, histologically or cytologically confirmed prostate adenocarcinoma and planned radical prostatectomy. Main exclusion criteria were any contraindication for performing a PET/MRI scan and patient's non-eligibility for the size of the PET/MRI gantry.

Each patient received a PET/MRI scan with [^{68}Ga]Ga-PSMA$^{HBED-CC}$ and 16β-[^{18}F]fluoro-5α-dihydrotestosterone prior to surgery. Scans were scheduled on 2 separate study days allowing a scan-free interval of at least 24 hours between the two scans. A blood sample prior to [18F]FDHT-PET scan was taken for the determination of serum testosterone and prostate-specific antigen (PSA) levels.

Up to 6 weeks after the first scan, subjects were admitted to the clinical ward at the Department of Urology and a radical prostatectomy was performed by a urologist following standardized procedures. Timing and indication of surgery was not influenced by study participation. Tumor tissue obtained during surgery was used for immunohistochemical analysis of AR and PSMA expression in addition to the routine pathological workup at the Department of Pathology.

PET/MRI Imaging

Radiosyntheses. All radiotracers for the study listed below were produced in-house at the Radiopharmacy Unit, Vienna General Hospital, applying standard procedures in accordance with the state of the art in radiopharmaceutical preparations. Quality control was performed according to the European Pharmacopoeia. For details of the radiosynthesis, refer to the supplemental material.

Imaging Protocols. All PET/MRI examination were conducted on a Biograph mMR (Siemens, Germany), consisting of PET detector integrated with a 3.0 T whole-body MRI scanner. Two different imaging protocols were used. At our hospital, every newly diagnosed prostate cancer patient receives a diagnostic [68Ga]PSMA-PET/MRI examination using a multiparametric MRI protocol with contrast enhancement to accurately evaluate the primary tumor and the prostate region (12). However, since [18F]FDHT PET is not yet established for routine clinical use at our institution and there are no previous studies using [18F]FDHT and PET/MRI scanners, the protocols described in previous studies regarding this tracer in metastatic castration-resistant prostate cancer were followed. For the clinic evaluation the most relevant MR-sequences of the pelvic region were acquired (7,14,15). The PET images were reviewed by two trained nuclear medicine physicians.

FDHT PET/MRI Protocols. The [18F]FDHT-PET/MRI examinations were performed 60 min after intravenous injection of 3 MBq per kg body weight 16β-[^{18}F]fluoro-5α-dihydrotestosterone. Static 10-min sinogram mode of the pelvis and 16-min partial body PET (skull base to knees) were performed with four bed positions, each with a 4-min sinogram mode. For details of the sequence parameters, refer to the supplemental material.

Reconstruction parameters for PET were: 3 iterations/21 subsets; summation of the 10 minutes pelvic acquisition for visual and semiquantitative analysis. MRI-based attenuation correction was applied using DIXON-VIBE sequences

comprising in- and opposed-phase as well as fat- and water-saturated images.

Ga-PSMA PET/MRI Protocols. For [68Ga]PSMA-PET/MRI studies, a 45-min dynamic list mode PET acquisition of the pelvis started immediately after the intravenous injection of 2 MBq/kg body weight [^{68}Ga]Ga-PSMA$^{HBED-CC}$. This followed by whole body PET (skull base to mid-thigh) performed with 4 bed positions, 4-min sinogram mode each. Reconstruction parameters for PET were: 3 iterations/ 21 subsets; summation of the last 10 minutes pelvic acquisition for visual and semiquantitative analysis. MRI-based attenuation correction was applied using DIXON-VIBE sequences comprising in- and opposed-phase as well as fat- and water-saturated images. For details of the sequence parameters, refer to the supplemental material.

To improve the image quality, especially of pelvic and abdomen images, forced diuresis with 20mg furosemide and Buscopan® 20mg were applied intravenously before the [^{68}Ga]Ga-PSMA$^{HBED-CC}$ application and all patients have received a bladder catheter.

PET Data Analysis. PET data were analyzed using HybridViewer 3D (Hermes Medical Solutions, Stockholm, Sweden) software. Anatomically exact regions of interest based on MRI data were defined. Semi-automated threshold-based volume of interest VOIs were generated in areas with focally increased [68Ga]PSMA or [18F]FDHT uptake and evaluated with respect to the following semi-quantitative data: maximal standardized uptake value (SUV_{max}), mean standardized uptake value (SUV_{mean}) and peak standardized uptake value (SUV_{peak}). A threshold of 90% of SUV_{max} corrected for local background was applied for semi-automated PET-imaging of both [68Ga]PSMA and [18F]FDHT. Background SUV_{mean} was measured in gluteus muscle for each subject separately ($SUV_{background}$). Ratios of tumor SUV to $SUV_{background}$ were calculated for SUV_{max}, SUV_{mean} and SUV_{peak}.

Immunohistochemical Analysis and Handling of Samples

Immunohistochemical (IHC) analysis was performed on tumor tissue at the Department of Pathology (Medical University of Vienna) using the automatic staining system VENTANA BenchMark ULTRA (Roche Tissue Diagnostics). For details of IHC analysis, refer to the supplemental material. Interpretation of marker expression was performed by the same qualified uropathologist. Membranous PSMA and nuclear AR receptor quantification for each sample was semi-quantitatively determined by a qualified uropathologist blinded to clinical data using a four-tiered system (0, 1+, 2+, 3+). All regions present on the

histological slide were evaluated. Based on the overall expression of said markers the rating “0” indicates no expression and “3+” the strongest expression. If heterogeneous AR or PSMA expression was present, the regions were separated into two regions with low versus high protein expression. Membranous and cytoplasmic PSMA expression as well as nuclear expression for AR were also quantitatively determined using the open source bioimage analysis software QuPath (v.0.3.0). The area chosen for analysis was spatially matched with the area of SUV_{max} detection in FDHT-PET imaging. For AR, the “positive cell detection” function was used to automatically detect positive stained cells in an area of 4 mm^2 based on the average 3,3'-Diaminobenzidine staining intensity within the nucleus and given as Diaminobenzidine optical density (OD) mean, ranging from 0-1 with a cutoff value of 0.05 to detect positive cells. To also account for the cell density in the marked area the sum of all Diaminobenzidine OD mean values (OD mean sum) was chosen for further analysis. For PSMA, a pixel classifier was trained after annotation of sample positive and negative areas. This pixel classifier was used to detect the positive staining area within the mentioned 4 mm^2 area. In the next step the average Diaminobenzidine staining intensity in this positive staining area was calculated and multiplied with the surface area to account for cell density.

Trial Endpoints and Statistical Analysis

The main outcome parameter was the correlation between tracer radiation dose normalized to injected dose, expressed as SUV and PSMA and AR protein expression levels in tissue samples assessed by IHC. Quantitative protein expression levels and the four-tiered ratings were correlated with SUV_{max}, SUV_{mean} and SUV_{peak} and the respective SUV to $SUV_{background}$ ratios. In case of heterogenous protein expression, the areas with stronger staining intensity spatially matched the areas of SUV detection and were therefore chosen for the correlation analysis. Linear correlation was investigated using the Pearson's Correlation Coefficient ® and reported with the 95% confidence interval (CI).

Statistical analysis was performed using a commercially available computer program (GraphPad Prism 9.3.1 for macOS, GraphPad Software, San Diego, California USA). All data collected are expressed as mean with standard deviation (SD) or median with interquartile range (IQR).

RESULTS

Demographics and Clinical Characteristics of Subjects

Between February 2020 and March 2021, ten patients with newly diagnosed PC were included in the study and completed all study procedures (table 1). None of the patients had received any hormonal cancer therapy. None of the patients had a testosterone level below the castration threshold of 0.5 ng/mL. Pathological workup of the tumor tissue revealed a median Gleason score of 8 (7-8).

PET Scans

The tumor detection rate of the [68Ga]PSMA-PET scan was 90% and 40% for the [18F]FDHT-PET scan. Representative Ga-PSMA- and [18F]FDHT-PET scans are shown in figure 1.

Measured SUVs in PC lesions for [68Ga]PSMA and [18F]FDHT are shown in figure 2. Mean SUV_{max} values of [68Ga]PSMA-PET and [18F]FDHT-PET were 17.0±15.0 and 3.4±0.5, respectively. Mean background SUV_{mean} measured in the gluteus muscle was 0.5±0.1 and 0.7±0.1 for [68Ga]PSMA- and [18F]FDHT-PET, respectively. Ratios of tumor SUV to background SUV are shown in table 2. For [68Ga]PSMA these were considerably higher compared to [18F]FDHT. The highest ratios were achieved for SUV_{max} with values of 34.9±24.8 and 4.8±1.2 for [68Ga]PSMA and [18F]FDHT, respectively.

Immunohistochemistry

The quantification results of the immunohistochemical staining of PSMA and AR in the tumor tissue are shown in table 3 and sample pictures of the staining are shown in figure 1. The semi-quantitative evaluation of the membranous staining intensity of PSMA yielded very homogenous results with values of 3+ for most subjects (90%). In contrast to this, the AR staining was rated with 1+ in two patients (20%), with 2+ in four patients (40%) and with 3+ in four patients (40%). Three patients (1, 5 and 6) demonstrated highly heterogeneous AR expression with areas showing negative and positive nuclear AR expression. For subject 5, areas with high AR expression showed considerably lower PSMA expression (supplemental figure 1). In this subject the missing AR staining was found especially in low differentiated, cribriform glands. However, this could not be observed in the other subjects. In contrast, in subject 6 AR staining was only visible in low differentiated, cribriform glands. The Gleason patterns within the different areas of the subjects did not show significant differences [subject 1: 7 (3+4); subject 5: 7 (3+4), subject 6: 8 (4+4)].

The mean PSMA Diaminobenzidine OD (± SD) measured with QuPath was 2257912 ± 1297251. The mean nuclear AR Diaminobenzidine OD (± SD) measured with QuPath was 3857 ± 2991.

Correlation

An overview of the different correlations is given in table 4. Correlation of imaging signals with the four-tiered rating was not investigated for PSMA since protein expression was high (rated with "3+") in all patients. For all investigated correlations, the $SUV_{max}/SUV_{background}$ ratio consistently yielded the strongest correlation with staining intensity.

A strong significant correlation between the AR expression and the FDHT $SUV_{max}/SUV_{background}$ ratio with correlation coefficients of r=0.72 (95% CI 0.17 to 0.93) for the optical density (figure 3) and r=0.80 (95% CI 0.34 to 0.95) for the four-tiered rating could be demonstrated.

In contrast, correlation between the PSMA optical density and the Ga-PSMA $SUV_{max}/SUV_{background}$ ratio was not significant (P-value=0.061) with a correlation coefficient of r=0.61 (95% CI -0.03 to 0.90) (figure 3).

DISCUSSION

A significant positive correlation between [18F]FDHT uptake in the PET scans and AR expression in cancer tissue could be demonstrated. For PSMA the PET/IHC correlation showed a positive trend but was not significant.

To our knowledge the present study is the first study that aimed to quantitatively assess whether [18F]FDHT and [68Ga]PSMA uptake in PET scans correlates with histopathological AR and PSMA expression.

The [18F]FDHT $SUV_{max}/SUV_{background}$ ratio showed a strong significant correlation (P-value=0.019, r=0.72) with AR optical density of the correlating tissue sample. Compared to previous studies in humans, lower [18F]FDHT SUVs were observed in the present study (*8,9*). Larson et al. performed [18F]FDHT PET scans in seven patients with PC and observed an average SUV_{max} of 5.28±2.57 (*8*). An even higher SUV_{max} of 7.46±3.37 was reported by Vargas et al. in 27 patients with PC (*9*). These values are 1.6- to 2.2-fold higher compared to the average SUV_{max} (3.4±0.5) observed in the present study. Presumably, the underlying reason for this is that for the present study patients were enrolled who did not receive any hormonal pre-therapy and therefore had physiological testosterone blood levels. It can be assumed that [18F]FDHT binding to ARs was competitively inhibited by endogenous dihydrotestosterone (DHT) leading to comparatively low [18F]FDHT uptake. In contrast, previous studies with [18F]FDHT only included patients with testosterone concentrations below the castration threshold (<50 ng/dL) (*7,8,14*). A finding that supports our theory was described by Larson et al. (*8*). The authors

performed a [18F]FDHT PET scan in castrated PC patients and rescanned two of the study subjects after administration of exogenous testosterone. In one of the two patients, the plasma DHT concentration was considerably higher prior to the second [18F]FDHT scan and tracer uptake also decreased substantially. In the other patient, tracer uptake was unchanged compared to the initial scan, probably because plasma DHT initially increased, but then decreased again prior to the [18F]FDHT scan.

Currently, there are two studies published, which investigated the correlation between [68Ga]PSMA uptake in PET and IHC PSMA expression. In the prospective study by Rüschoff et al., IHC staining intensity was only determined semiquantitatively, according to the four-tiered rating system. A positive trend was described for the membraneous and cytoplasmatic PSMA expression, which did not reach significance (*15*). Similar to the study by Rüschoff et al., in the retrospective study by Woythal et al. a four-tiered rating system was used for PSMA staining intensity (*16*). Woythal et al. did not discriminate between membranous and cytoplasmatic PSMA expression and they were able to demonstrate a significant correlation between SUV_{max} and the immunoreactive score (IRS) which incorporates staining intensity and percentage of positive cells (P-value<0.001). Unfortunately, the authors do not report the correlation between SUV_{max} and staining intensity. The patient characteristics of the study by Woythal et al. were comparable to the present study with a mean Gleason

Score of 7.9, but the sample size was larger (31 primary PC patients). In the present study SUV_{max} and staining intensity were positively correlated, but without statistical significance (r=0.6; P-value=0.068). Compared to the studies mentioned above, we used a more refined, granular and objective method for staining intensity assessment. Unfortunately, membranous and cytoplasmatic PSMA expression could also not be discriminated in our study due to artifacts generated by the high cytoplasmatic background PSMA staining in the automatic cell detection using QuPath. Therefore, the software was not able to reliably differentiate between membranous and cytoplasmatic expression. Interestingly, the correlation between PSMA optical density and the [68Ga]PSMA $SUV_{max}/SUV_{background}$ ratio was not significant, yet a positive correlation trend could be observed (figure 3). The small sample size may account for this lack of significance. However, the present study was designed as an exploratory pilot study and therefore only 10 patients were included.

The tumor detection rate was 40% in the [18F]FDHT-PET scans and 90% in the [68Ga]PSMA-PET scans. In line with this finding, SUV_{max} values for [68Ga]PSMA were about seven-fold higher compared to [18F]FDHT (34.9±24.8 vs. 4.8±1.2, respectively). Despite the low detection rate, ratios of [18F]FDHT cancer SUV to background SUV were always above 1, indicating increased binding of FDHT in cancer tissue (table 2). However, the SUV ratios were not high enough to be identified as tumor-positive areas. This explains that a significant correlation

between [18F]FDHT $SUV_{max}/SUV_{background}$ ratio and AR optical density could be observed, despite the low tumor detection rate.

In future studies the correlation between [18F]FDHT SUVs and AR expression in patients with low testosterone levels should be examined to investigate the hypothesis that endogenous androgens antagonize [18F]FDHT. In these patients the correlation of [18F]FDHT with AR expression might be more pronounced and is of particular clinical importance, since PC is usually progressed in these patients.

Another interesting finding of our study was the highly heterogeneous AR expression in three subjects. Magi-Galluzzi et al. performed a retrospective analysis of 40 PC samples and observed decreasing AR staining with increasing Gleason grade (*17*). To investigate if the different regions in our subjects indicate different foci of aggressiveness, we determined the Gleason patterns for the different regions of AR expression. However, no significant differences could be observed. Others have observed that AR positive cells were also PSMA positive (*18*). We did not observe this trend. On the contrary, in one subject areas with higher AR expression showed lower PSMA expression. In consequence, no correlation between morphology and expression pattern can be derived from these findings and the influence of fixation artifacts in preanalytics cannot be excluded.

As mentioned above, a limitation of the present study was the small sample size. For a more robust statistical analysis a higher sample size would have been preferable, but due to the exploratory character of the study only 10 patients were included. In addition, the effects of hormonal therapy on [18F]FDHT uptake and the correlation of [18F]FDHT uptake with therapeutic response remain to be investigated in future longitudinal studies.

CONCLUSION

The findings of our study suggest that [18F]FDHT-PET scans may be useful for monitoring AR expression and alterations of AR expression during PC treatment. Knowledge of changes in AR expression during disease progression could help clinicians recognize imminent resistance to therapy and improve patient outcomes.

DISCLOSURE STATEMENT

No potential conflicts of interest relevant to this article exist.

ACKNOWLEDGEMENTS

The authors thank Neydher Berroterán-Infante for his help in establishing the 16β-[^{18}F]fluoro-5α-dihydrotestosterone synthesis.

KEY POINTS

Question: Can PET imaging be used as a substitute for immunohistochemical analysis of tumor samples in patients with newly diagnosed PC?

Pertinent findings: This prospective, explorative clinical study in 10 patients with newly diagnosed prostate cancer investigated the correlation between imaging signals of [^{68}Ga]Ga-PSMA$^{HBED-CC}$ and [^{18}F]-fluoro-5α-dihydrotestosterone ([18F]FDHT) and the protein expression of their corresponding target structures (PSMA and androgen receptor). The results suggest that [18F]FDHT-PET scans may be useful for monitoring AR receptor expression and alterations of AR expression during prostate cancer treatment.

Implications for patient care: Monitoring AR expression during disease progression could help clinicians recognize imminent resistance to therapy and thereby improve patient outcomes.

REFERENCES

1. Bray F, Ferlay J, Soerjomataram I, Siegel RL, Torre LA, Jemal A. Global cancer statistics 2018: GLOBOCAN estimates of incidence and mortality worldwide for 36 cancers in 185 countries. *CA Cancer J Clin.* 2018;68:394-424.

2. Zhai Z, Zheng Y, Li N, et al. Incidence and disease burden of prostate cancer from 1990 to 2017: Results from the Global Burden of Disease Study 2017. *Cancer.* 2020;126:1969-1978.

3. Craft N, Sawyers CL. Mechanistic concepts in androgen-dependence of prostate cancer. *Cancer Metastasis Rev.* 1998;17:421-427.

4. Visakorpi T, Hyytinen E, Koivisto P, et al. In vivo amplification of the androgen receptor gene and progression of human prostate cancer. *Nat Genet.* 1995;9:401-406.

5. Wang L, Paller CJ, Hong H, De Felice A, Alexander GC, Brawley O. Comparison of systemic treatments for metastatic castration-sensitive prostate cancer: a systematic review and network meta-analysis. *JAMA Oncol.* 2021;7:412-420.

6. Koivisto P, Kononen J, Palmberg C, et al. Androgen receptor gene amplification: a possible molecular mechanism for androgen deprivation therapy failure in prostate cancer. *Cancer Res.* 1997;57:314-319.

7. Fox JJ, Gavane SC, Blanc-Autran E, et al. Positron Emission Tomography/Computed Tomography-based assessments of androgen receptor expression and glycolytic activity as a prognostic biomarker for metastatic castration-resistant prostate cancer. *JAMA Oncol.* 2018;4:217-224.

8. Larson SM, Morris M, Gunther I, et al. Tumor localization of 16beta-18F-fluoro-5alpha-dihydrotestosterone versus 18F-FDG in patients with progressive, metastatic prostate cancer. *J Nucl Med.* 2004;45:366-373.

9. Vargas HA, Kramer GM, Scott AM, et al. Reproducibility and repeatability of semiquantitative (18)F-fluorodihydrotestosterone uptake metrics in castration-resistant prostate cancer metastases: a prospective multicenter study. *J Nucl Med.* 2018;59:1516-1523.

10. Perera M, Papa N, Roberts M, et al. Gallium-68 prostate-specific membrane antigen Positron Emission Tomography in advanced prostate cancer-updated diagnostic utility, sensitivity, specificity, and distribution of prostate-specific membrane antigen-avid lesions: a systematic review and meta-analysis. *Eur Urol.* 2020;77:403-417.

11. Hofman MS, Lawrentschuk N, Francis RJ, et al. Prostate-specific membrane antigen PET-CT in patients with high-risk prostate cancer before curative-intent surgery or radiotherapy (proPSMA): a prospective, randomised, multicentre study. *Lancet.* 2020;395:1208-1216.

12. Grubmuller B, Baltzer P, Hartenbach S, et al. PSMA ligand PET/MRI for primary prostate cancer: staging performance and clinical impact. *Clin Cancer Res.* 2018;24:6300-6307.

13. Orevi M, Shamni O, Zalcman N, et al. [(18)F]-FDHT PET/CT as a tool for imaging androgen receptor expression in high-grade glioma. *Neurooncol Adv.* 2021;3:vdab019.

14. Rathkopf DE, Morris MJ, Fox JJ, et al. Phase I study of ARN-509, a novel antiandrogen, in the

treatment of castration-resistant prostate cancer. *J Clin Oncol.* 2013;31:3525-3530.

15. Ruschoff JH, Ferraro DA, Muehlematter UJ, et al. What's behind (68)Ga-PSMA-11 uptake in primary prostate cancer PET? Investigation of histopathological parameters and immunohistochemical PSMA expression patterns. *Eur J Nucl Med Mol Imaging.* 2021;48:4042-4053.

16. Woythal N, Arsenic R, Kempkensteffen C, et al. Immunohistochemical validation of PSMA expression measured by (68)Ga-PSMA PET/CT in primary prostate cancer. *J Nucl Med.* 2018;59:238-243.

17. Magi-Galluzzi C, Xu X, Hlatky L, et al. Heterogeneity of androgen receptor content in advanced prostate cancer. *Mod Pathol.* 1997;10:839-845.

18. Batra JS, Pienta KJ, Pomper MG, Gorin MA, Rowe SP. Can the interplay between androgen signaling and PSMA expression be leveraged for theranostic applications? *Transl Androl Urol.* 2019;8:S263-s264.

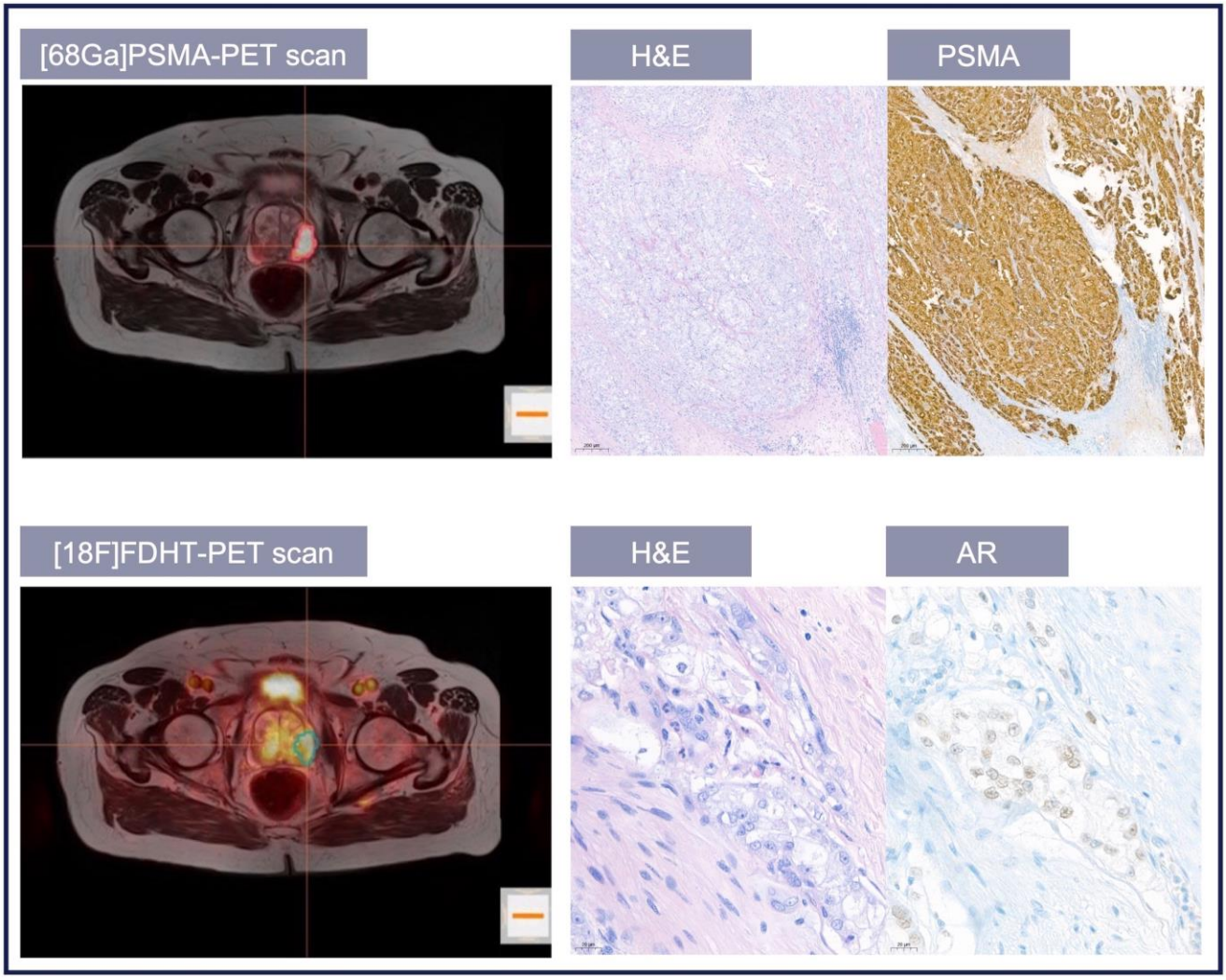

Figure 1 – Example PET images and immunohistochemical (IHC) stains of one study patient. IHC images of prostate-specific membrane antigen (PSMA) staining and androgen receptor (AR) staining are magnified 5-fold and 40-fold, respectively. $SUV_{max}/SUV_{background}$ ratio for the Ga-PSMA-PET scan was 14.3 and for the FDHT-PET scan 5.0. The staining of the tissue samples shows strong PSMA expression, but weak AR expression.

H&E = Hematoxylin and Eosin stain; [^{68}Ga]Ga-PSMA$^{HBED-CC}$ PET/MRI = Ga-PSMA-PET scan; [^{18}F]-fluoro-5α-dihydrotestosterone PET/MRI = FDHT-PET scan

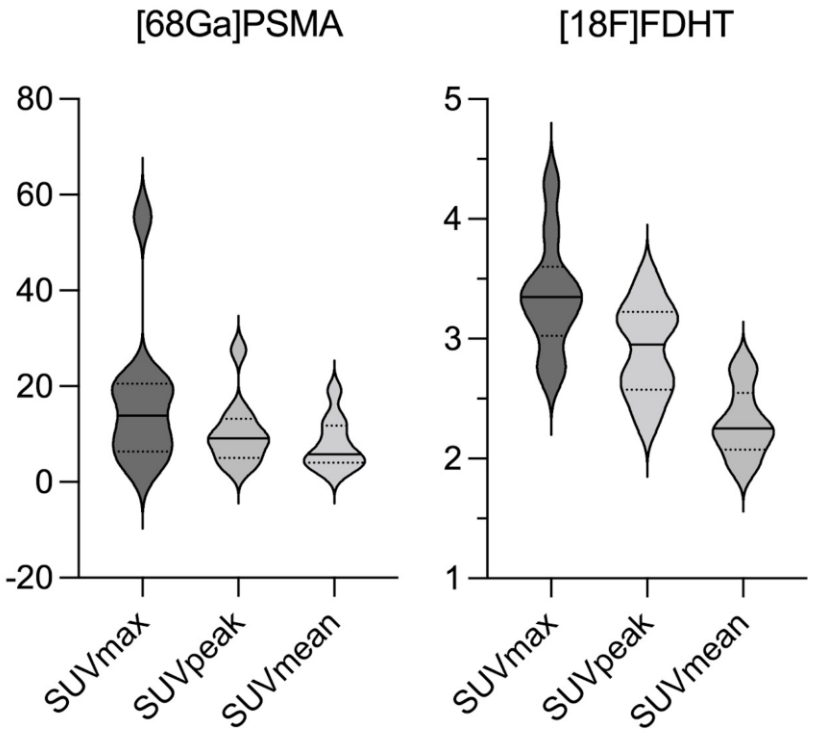

Figure 2 – Standardized uptake values (SUV) of PET scans in prostate cancer tissue for [^{68}Ga]Ga-PSMA$^{HBED-CC}$ (PSMA) and [^{18}F]-fluoro-5α-dihydrotestosterone (FDHT) as SUVmax, SUVpeak and SUVmean.

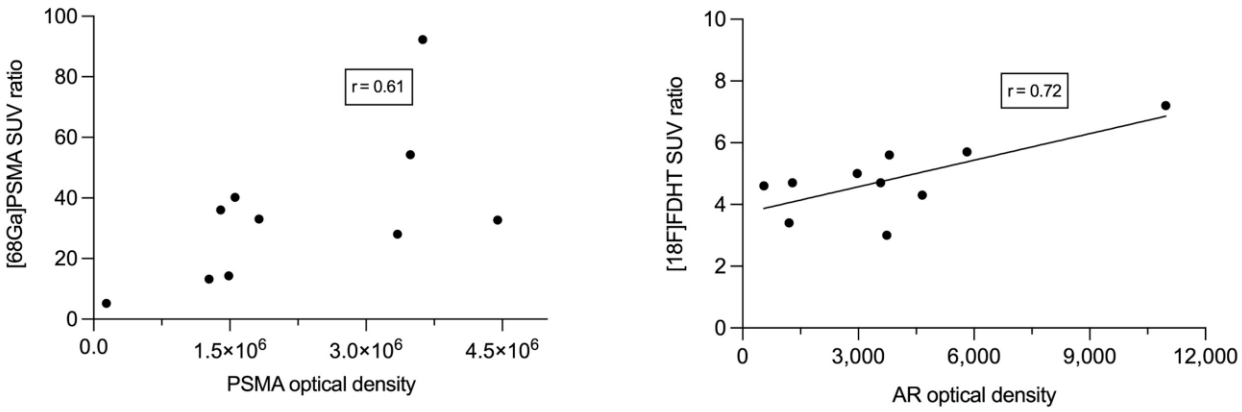

Figure 3 – Correlation graph between the $SUV_{max}/SUV_{background}$ ratio (SUV ratio) and the prostate-specific membrane antigen (PSMA) and androgen receptor (AR) Diaminobenzidine optical density (OD). The straight line represents the linear regression line. PSMA OD was calculated as PSMA Diaminobenzidine OD mean * surface area and AR OD is the AR Diaminobenzidine OD mean sum.

Table 1 – Patient characteristics and pathological tumor characteristics.

Characteristic	
Number of subjects	10
Age (years) [a]	60 (54-67)
BMI (m^2/kg) [a]	25.9 (25-27)
PSA (µg/L) [b]	8.8 ± 4.1
Testosterone (ng/mL) [b]	3.4 ± 1.2
Gleason Score[a]	8 (7-8)
Pathological stage (%)	
pT2	3 (30%)
pT3a	3 (30%)
pT3b	4 (40%)

[a]median (IQR), [b]mean ± standard deviation

Table 2 - Ratios of tumor standardized uptake values (SUV) to background SUV (SUV_{mean} measured in gluteus muscle) for PSMA- and FDHT-PET scans.

	Ga-PSMA	FDHT
SUV_{max}/BG	34.9±24.8	4.8±1.2
SUV_{peak}/BG	22.3±14.6	4.1±0.8
SUV_{mean}/BG	18.1±17.1	3.3±0.8

Table 3 – Immunohistochemical staining intensity of prostate-specific membrane antigen (PSMA) and androgen receptor (AR) determined by a qualified uropathologist (four-tiered rating) and by the software QuPath (3,3'-Diaminobenzidine optical density). PSMA optical density (OD) was calculated as PSMA Diaminobenzidine OD mean * surface area and AR optical density is the AR Diaminobenzidine OD mean sum.

	Uropathologist (four-tiered rating)		QuPath (optical density)	
subject	PSMA	AR	PSMA (10^6)	AR (10^3)
1	3+	0, 1+	1.398	1.203
2	3+	3+	1.557	3.804
3	3+	3+	3.487	5.815
4	3+	3+	1.272	4.660
5	3+, 2+	0, 3+	1.820	10.968
6	3+	0, 2+	3.625	1.291
7	3+	2+	1.487	2.967
8	3+	1+	3.345	3.737
9	3+	2+	4.449	3.575
10	3+	2+	0.141	0.552

Table 4 - Pearson's Correlation Coefficient (r) with the 95% confidence interval (CI) and the P-value for the correlation of the optical density and the four-tiered rating with different imaging parameters. Correlation to the four-tiered rating was not investigated for prostate-specific membrane antigen since protein expression was rated the same in all patients.

	Prostate-specific membrane antigen		**Androgen receptor**			
	optical density		optical density		four-tiered rating	
Imaging parameter	Pearson r (CI)	P-value	Pearson r (CI)	P-value	Pearson r (CI)	P-value
SUV_{max}	0.60 (-0.05 to 0.89)	0.068	0.64 (0.02 to 0.91)	0.045	0.73 (0.19 to 0.93)	0.016
SUV_{mean}	0.37 (-0.34 to 0.81)	0.298	0.17 (-0.52 to 0.72)	0.644	0.10 (-0.57 to 0.68)	0.790
SUV_{peak}	0.56 (-0.11 to 0.88)	0.096	0.34 (-0.37 to 0.80)	0.343	0.28 (-0.42 to 0.77)	0.427
$SUV_{max}/SUV_{background}$	0.61 (-0.03 to 0.90)	0.061	0.72 (0.17 to 0.93)	0.019	0.80 (0.34 to 0.95)	0.005
$SUV_{mean}/SUV_{background}$	0.09 (-0.57 to 0.68)	0.814	0.45 (-0.25 to 0.84)	0.193	0.47 (-0.23 to 0.85)	0.176
$SUV_{peak}/SUV_{background}$	0.38 (-0.33 to 0.81)	0.285	0.64 (0.02 to 0.91)	0.047	0.66 (0.05 to 0.91)	0.038

Graphical Abstract

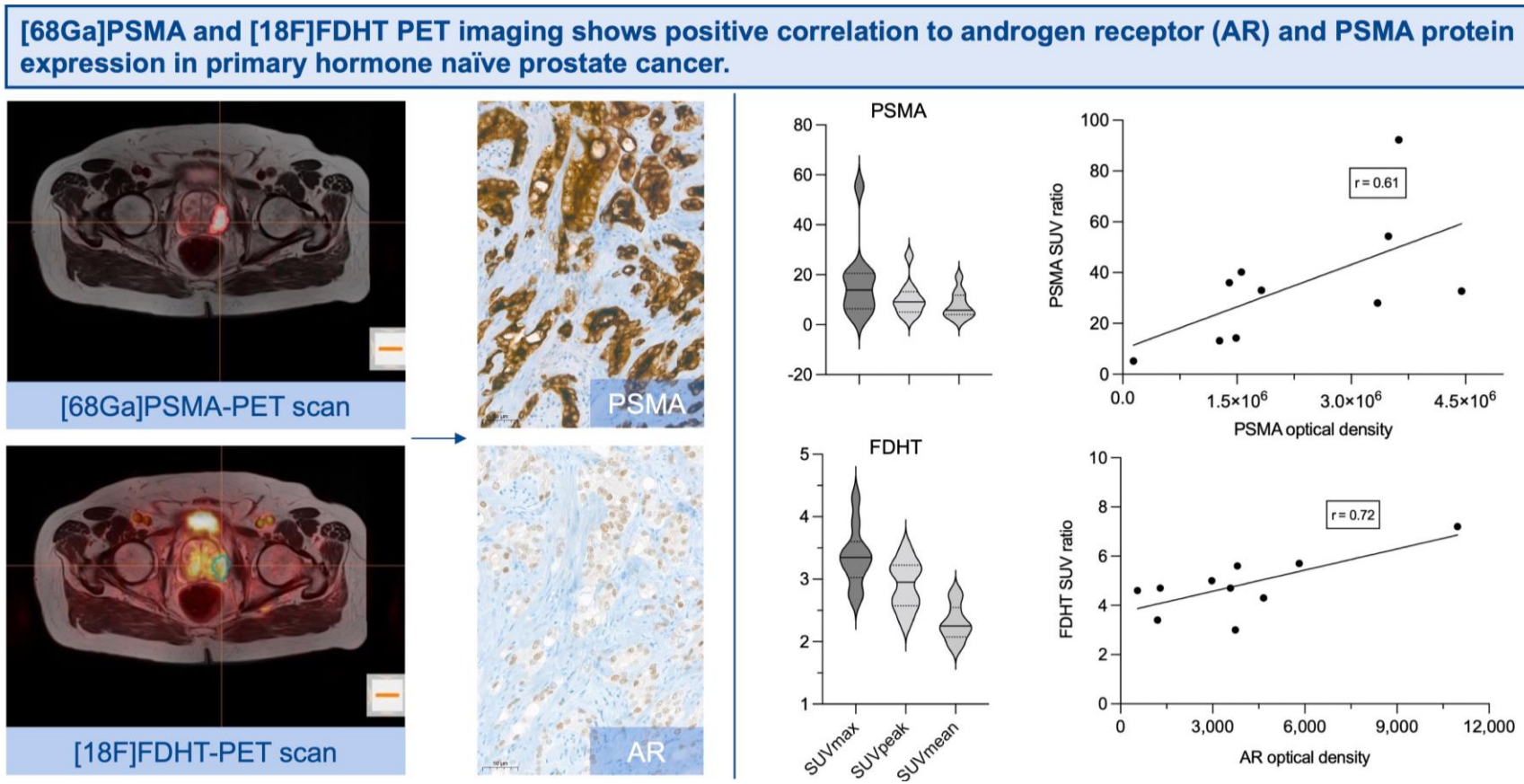

Supplement

Radiosyntheses

All radiotracers for the study listed below were produced in-house at the Radiopharmacy Unit, Vienna General Hospital, applying standard procedures in accordance with the state of the art in radiopharmaceutical preparations. Quality control was performed according to the European Pharmacopoeia. 25 µg PSMA HBED-CC was labelled in acetate buffer at room temperature for 5 min using a dedicated kit (Telix Pharmaceuticals Ltd.) and 1.1 mL generator eluate (Galli Eo™, IRE Elit) under aseptic conditions. The obtained product [68Ga]Ga-PSMA HBED-CC ([68Ga]Ga-PSMA-11) was used without further purification. The radiosynthesis of 16β-[18F]fluoro-5α-dihydrotestosterone was performed as previously described with some modifications using an automated synthesizer (TracerLab FXFN, Nuclear Interface platform, GE Healthcare).(14) In brief, [18F]fluoride was produced on-site via 18O(p,n)18F reaction (GE PET trace, GE Medical Systems). After azeotropic drying in the presence of Kryptofix 2.2.2 and potassium carbonate, [18F]fluoride reacted with the precursor 16α- [[(trifluoromethyl)sulfonyl]oxy]-3,3-(ethylenedioxy)androstan-17-one (GMP-grade, ABX GmbH) in acetonitrile (40°C, 10 min). The crude product was separated from the reaction mixture by solid phase extraction (Sep-Pak® tC18 Plus), washed and eluted with ethanol to a second reaction vessel. Sodium borohydride was added for reduction and then the protective groups were removed by acid hydrolysis (2 N HCl, 85°C). After neutralization, the crude product was purified by radio-HPLC and solid phase extraction and subsequently formulated in physiological saline containing < 10% ethanol.

Immunohistochemical analysis

PSMA IHC was performed using a Rabbit Anti-Human PSMA Antibody (AC-0160; monoclonal [clone EP192]; Epitomics, Inc.: Burlingame, California, USA). AR IHC was performed using a Mouse Anti-Human AR Antibody (M3562; monoclonal [clone AR441]; DAKO, Agilent Technologies: Santa Clara, California, USA). Interpretation of marker expression in all tissue samples was performed by the same qualified uropathologist using high resolution scans performed with the Pannoramic 250 Flash II digital scanner (3DHistech) at 40x magnification.

Imaging protocols – sequence parameters

FDHT PET/MRI

For the integrated 3T MRI following sequences and parameters were performed: Pelvis: T2w turbo spin echo (tse) axial, in-plane resolution: 0.8x0.8x5mm; Acq. Matrix 235x512 FoV phase: 262.5mm; TR: 3600ms; TE: 103ms. T1w turbo spin echo (tse) coronal: Matrix size: 346x385, in-plane resolution: 0.9x0.9x5mm FoV phase: 350mm; TR: 600ms; TE: 12ms. Diffusion weighted imaging: Acq. Matrix size: 108x192, in-plane resolution: 2.0x2.0x5mm; FoV: 180mm; with b-values: 0 and 600s/mm²; TR: 9200ms; TE: 85ms. Partial body MRI simultaneous with PET: T2w HASTE: Matrix size: 256x256, in-plane resolution: 1.5x1.5x6mm; FoV: 380mm; TR: 1400ms; TE: 121ms. T1 VIBE Dixon: Matrix

size: 175x320, in-plane resolution: 1.3x1.3x3mm; FoV: 320mm; TR: 4.02ms; TE: 1.23/2.46ms. Diff. stir: Acq. Matrix 105x168, b values 50 and 800, TR: 600ms; TE 68ms.

Ga-PSMA PET/MRI

The integrated 3T MRI was performed with the following sequences and parameters: T2 tse tra pelvis: Matrix size 235x512, in-plane resolution 0.8x0.8x5mm, Acq. Matrix 235x400, TR 3100ms, TE 106. T2 tse tra p2: Matrix size 320x320, in-plane resolution 0.6x0.6x3.5, FoV 200mm, TR 7500ms, TE 101ms. T2 space tra p2: Matrix 300x320, in-plane resolution 0.7x0.7x1mm; FOV 291x320mm, TR 1600ms, TE 88ms. T2 tse sag p2: Matrix 310x320, in-plane resolution 0.6x0.6x3.5mm, FoV 200mm, TR 7500ms, TE 101ms. T2 tse cor p2 320: Matrix 320x320, in-plane resolution 0.6x0.6x3.5 mm, FoV 200mm, TR 7500ms, TE 101ms. Diffusion weighted imaging: ep2d diff b0 800 tra p2: Matrix size 132x132, in-plane resolution 1.5x1.5x3.5mm, FoV 200mm, TR 4200ms, TE 87ms. T1 vibe tra dyn dixon 2 means: Matrix 154x192, in-plane resolution 1.4x1.4x3.5mm, FOV 260mm, TR 4.75ms, TE1 1.34ms and TE2 2.57ms. Whole body MRI simultaneous with PET: T1 vibe fs tra GK KM: Matrix size 195x320, in-plane resolution 1.2x1.2x3mm, FOV 380, TR 4.56ms, TE 2.01. T2w HASTE: Matrix size: 256x256, in-plane resolution 1.5x1.5x6mm, FoV 380mm, TR 1400ms, TE 121ms.

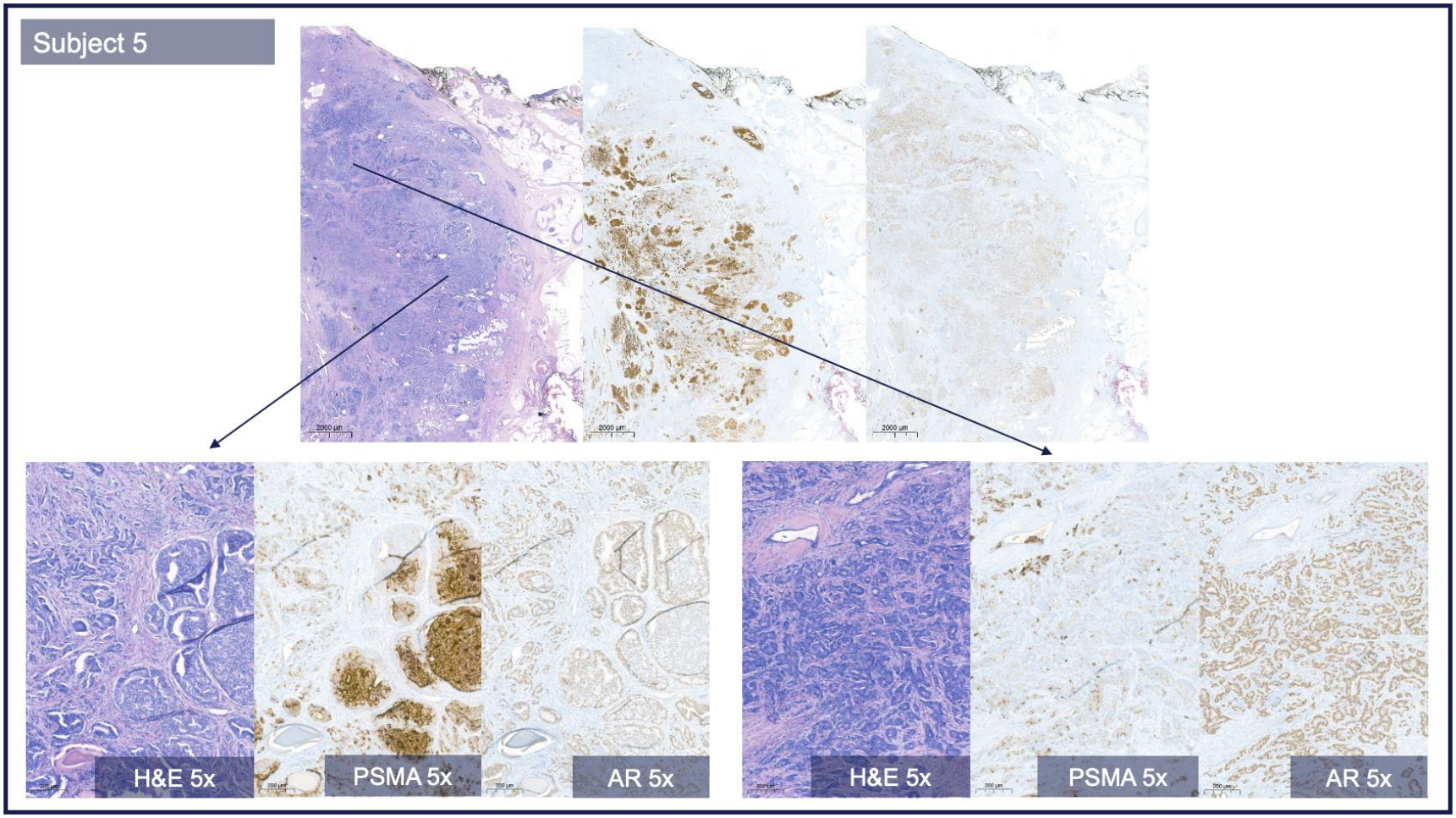

Supplemental figure 1 - Immunohistochemical (IHC) stains of subject 5. Staining images are magnified 5-fold. This figure shows a tissue specimen with heterogeneous AR and PSMA expression in two distinct morphological areas. On the left magnification, there is no AR expression in the center of the cribriform glands, but strong PSMA expression (rated with “3+”). On the right magnification the glands show strong AR expression (rated with “3+”), while PSMA stains weaker (rated with “2+”) and even partially negative.

H&E = Hematoxylin and Eosin stain; PSMA = prostate-specific membrane antigen, AR = androgen receptor